



1 **Multi-model ensemble projection of global dust cycle by the**
2 **end of 21st century using CMIP6 data**

3

4 **Yuan Zhao¹, Xu Yue¹, Yang Cao², Jun Zhu¹, Chenguang Tian¹, Hao Zhou²,**
5 **Yuwen Chen¹, Yihan Hu¹, Weijie Fu¹ and Xu Zhao¹**

6

7 ¹ Jiangsu Key Laboratory of Atmospheric Environment Monitoring and Pollution
8 Control, Collaborative Innovation Center of Atmospheric Environment and Equipment
9 Technology, School of Environmental Science and Engineering, Nanjing University of
10 Information Science & Technology (NUIST), Nanjing, 210044, China

11 ² Climate Change Research Center, Institute of Atmospheric Physics, Chinese Academy
12 of Sciences, Beijing, 100029, China

13

14

15 Corresponding author: Xu Yue (Email: yuexu@nuist.edu.cn)

16

17



18

19

Abstract

20 As a natural aerosol with the largest emissions on land, dust has important impacts
21 on atmospheric environment and climate systems. Both the emissions and transport of
22 dust aerosols are tightly connected to meteorological conditions and as a result are
23 confronted with strong modulations by the changing climate. Here, we project the
24 changes of global dust emissions and loading by the end of the 21st century using an
25 ensemble of model outputs from the Coupled Model Intercomparison Project version 6
26 (CMIP6) under four Shared Socioeconomic Pathways (SSPs). Based on the validations
27 against site-level observations, we select 5 out of 10 models and estimate an ensemble
28 global dust emission of 3311 Tg a⁻¹ (1Tg = 10¹²g) at present day, in which 75% is dry
29 deposited and 25% is wet deposited. Compared to 2005-2014, global dust emissions
30 show varied responses with a reduction of 15.8 Tg a⁻¹ under the SSP3-7.0 scenario but
31 increased emissions up to 53.4 Tg a⁻¹ under the SSP5-8.5 scenario at 2090-2099. For
32 all scenarios, the most significant increase of dust emissions appears in North Africa
33 (0.4%-4.7%) due to the combined effects of reduced relative humidity and precipitation
34 but strengthened surface wind. In contrast, all scenarios show decreased emissions in
35 central Asia and Taklimakan (-0.6% to -20%) and Middle East (0 to -2.8%) because of
36 the increased precipitation but decreased wind speed regionally. The dust loading
37 shows uniform increases over North Africa (1%-12.5%) and the downwind Atlantic
38 following the increased emissions, but decreases over East Asia (-3.4% to -15.2%) and
39 the downwind Pacific due to enhanced local precipitation that promotes wet deposition.
40 As a result, global dust loading will increase by 2.1%-9.3% at the end of the 21st century
41 under different climate scenarios, suggesting a likely strengthened radiative and
42 climatic perturbations by dust aerosols in a warmer climate.

43

44 **Keywords:** CMIP6, dust emissions, concentrations, climate change, ensemble
45 projection

46

47



48 **1 Introduction**

49 Dust aerosol is one of the major air pollutants with strong climatic and
50 environmental effects. Suspended dust aerosols can absorb and scatter solar radiation,
51 and act as condensation nuclei so as to change the cloud optical properties (Tegen et al.,
52 2004; Penner et al., 2006; Forster et al., 2008). Dust deposition can change the albedo
53 of snow and ice and transport mineral elements to the ocean (Jickells et al., 2005;
54 Mahowald et al., 2005; Wittmann et al., 2017). Furthermore, strong dust storms present
55 as a serious threat to human society by reducing road visibility that influences traffic
56 safety (Middleton, 2017), carrying bacteria and viruses that affects public health
57 (Goudie, 2014), and reducing crop yields that endangers the food supply (Stefanski and
58 Sivakumar, 2009). In light of the great impacts of dust on climate and environment, it
59 is of significant importance to study the spatiotemporal characteristics and future
60 changes of global dust aerosols.

61 The dust cycle consists of three major processes including emission, transport, and
62 deposition (Schepanski, 2018), which are mainly related to meteorological conditions,
63 such as precipitation, humidity, surface wind speed, and turbulent mixing (Liu et al.,
64 2004; Shao et al., 2011; Csavina et al., 2014). Low humidity and/or strong surface wind
65 are in favor of dust emissions (Csavina et al., 2014). Atmospheric humidity has a tight
66 coupling effect with soil moisture, which controls the threshold of friction velocity and
67 dust emission intensity (Munkhtsetseg et al., 2016). Strong winds and the associated
68 pressure systems promote the momentum of surface layer and consequently increase
69 dust mobilizations (Li et al., 2022). The transport of dust aerosols is related to
70 atmospheric circulation and turbulent mixing, which determine the horizontal and
71 vertical distribution of dust aerosol particles, respectively (Zhang et al., 2014;
72 Fernandes et al., 2020). The deposition process includes dry and wet settlement, in
73 which the dry deposition is an effective way to remove large particles while wet
74 deposition dominates the removal of fine particles (Breuning-Madsen and Awadzi,
75 2005; Yue et al., 2009). Therefore, the spatiotemporal variations of dust aerosols are
76 closely related to meteorological factors.

77 Climate change exerts significant impacts on the global dust cycle. A study using
78 the RegCM3 model showed that dust emissions and the column burden would increase
79 respectively by 2% and 14% in eastern Asia at 2091-2100 relative to 1991-2000 (Zhang
80 et al., 2016). In contrast, the earlier study projected the reductions of dust emissions by
81 26% using the ECHAM4-OPYC model and 19% using the HADCM3 model in the
82 same region by the midcentury (Tegen et al., 2004). Compared to these studies based
83 on 1-2 models, the ensemble projections using multiple models from the Climate Model



84 Inter-comparison Project (CMIP) showed great potentials of indicating the uncertainties
85 in the estimate of global dust cycle. Wu et al. (2020) evaluated 15 dust models in CMIP
86 phase 5 (CMIP5) and found that the uncertainty was relatively small for the dust belt
87 extending from North Africa to East Asia, but the uncertainties in other regions such as
88 Australia and North America were large. Based on the multi-model ensemble from
89 CMIP5 data, Pu and Ginoux (2018) estimated an increase of dust optical depth in
90 central Arabian Peninsula and a decrease over northern China in the late half of the 21st
91 century under a strong warming scenario. Zong et al. (2021) also projected that dust
92 emissions would decrease in East Asia by the end of 21st century under the same climate
93 scenario. However, the different features of future global dust cycles and the related
94 drivers under varied climate scenarios remain unclear.

95 Compared to CMIP5 models, more dust emission schemes are coupled with
96 dynamic vegetation in the CMIP phase 6 (CMIP6) models to optimize land surface
97 emission processes (Zhao et al., 2022). However, such improvement may instead
98 amplify the uncertainties of dust simulations, because the predicted vegetation change
99 may be inconsistent with the observed tendencies (Wu et al., 2020). As a result, it is
100 important to validate the simulated present-day dust cycle before the application of
101 different models in the future projection (Aryal and Evans, 2021). In this study, we
102 project the future changes in global dust cycles by the end of 21st century under four
103 different climate scenarios based on the multi-model ensemble mean from CMIP6
104 models. We select a total of 10 climate models providing dust emissions, depositions,
105 and concentrations for all the four scenarios and validate the simulated near-surface
106 dust concentrations at 18 ground sites. The models with reasonable performance are
107 selected to project future changes in dust emissions and loadings by the years 2090-
108 2099 relative to the present day (2005-2014). The changes in associated meteorological
109 conditions are further explored to identify the main causes of the changes in the global
110 dust cycle.

111

112 **2 Methods and data**

113 2.1 Model data

114 We select all available CMIP6 models providing complete variables of dust cycle
115 (emission, dry/wet deposition, and concentration) and the associated meteorology
116 (surface wind, relative humidity, precipitation) for both present day and four future
117 scenarios under the Shared Socioeconomic Pathways (SSPs) of SSP1-2.6, SSP2-4.5,



118 SSP3-7.0, and SSP5-8.5, which represent future climate with the low to high
119 anthropogenic radiative forcings. A total of 10 models with different spatial resolutions
120 are selected, including CESM2-WACCM, CNRM-ESM2-1, GFDL-ESM4, INM-CM4-
121 8, INM-CM5-0, MIROC6, MIROC-ES2L, MRI-ESM2-0, NorESM2-LM, UKESM1-
122 0-LL (Table 1). Different models may have varied numbers of ensemble runs for dust
123 cycle variables (Table S1). To facilitate the comparison, we select r1i1p1f1 for all
124 models but r1i1p1f2 for models without r1i1p1f1. To facilitate the model validation and
125 inter-comparison, we interpolate all model data with different spatial resolution to the
126 same of $1^\circ \times 1^\circ$. We use the average data from 2005 to 2014 to indicate conditions at
127 present day and that from 2090 to 2099 as the future period. We project the changes in
128 dust cycle using the multi-model ensemble median (MEM) values between future
129 and present day, and explore the causes of changes by linking the simulated dust cycle
130 with meteorological variables from individual models.

131

132 2.2 Measurement data

133 We use dust concentrations observed at 18 ground sites operated by University of
134 Miami to validate dust concentrations at the lowest level of the 10 models. All these
135 sites are located on the islands with 7 in the Atlantic, 7 in the Pacific, 3 in the Southern
136 Ocean, and 1 in the Indian Ocean. Most of these sites were built near the dust source
137 regions with the longest period of 17 years. Although the observed data are not
138 continuous at all sites, they provide the most valuable spatiotemporal information of
139 global dust concentrations and have been widely used in the evaluations of dust models
140 (Ginoux et al., 2001; Yue et al., 2009; Wu et al., 2020). By comparing with these
141 observations, we select 5 out of 10 climate models capturing the reasonable features
142 and magnitude of dust distribution for the future projections.

143

144 2.3 Dust emission schemes

145 The vertical emission flux F_i for a specific dust size bin i in most of climate models
146 can be derived using the generic equation:

$$147 \quad F_i = C \cdot \rho_d \cdot E \cdot f_m \cdot \alpha \cdot M_i \quad (1)$$

148 Here, C is a tunable parameter set to derive the reasonable dust climatology in
149 individual models. ρ_d is the density of dust particle. E is the impetus composed of
150 wind friction speed (U_f) above the threshold values (U_t) for saltation. The value of U_t



151 is dependent on soil moisture. f_m is the erodibility potential of bare soil suitable for
152 dust mobilization, which is usually parameterized as the cover fraction of a grid cell
153 excluding snow, ice, lake, and vegetation. α is sandblasting mass efficiency related to
154 clay fraction (%clay). M_i is the mass distribution of the specific dust size bin i . The
155 detailed parameterizations for each component of Equation (1) are shown for 5 selected
156 models in Table 2. In general, the main factors influencing dust emissions include wind
157 friction velocity, threshold wind speed, soil moisture, clay content, soil bareness, and
158 dust particle size. These variables are used either as individual factors or in multiple
159 components of Eq. 1. For example, in CESM2-WACCM, NorESM2-LM, and
160 UKESM1-0-LL, the clay fraction is used to calculate both sandblasting mass efficiency
161 and the threshold of wind friction speed (Lawrence et al., 2019). In CNRM-ESM2-1,
162 f_m , soil moisture, and %clay are combined to calculate U_t rather than acting as
163 individual components of F_i (Zakey et al., 2006).

164

165 **3 Results**

166 **3.1 Model validations**

167 Fig. 1a shows the spatial distribution of ground-based sites for dust observations.
168 These sites cover a wide range of oceanic areas with different distances to source
169 regions. Compared to observed concentrations, the simulations yield correlation
170 coefficients (R) of 0.11–0.89 for 10 climate models, among which 7 models show R of
171 higher than 0.8. The normalized standard deviations (NSD, standard deviation of the
172 model divided by that of the observations) range from 0.1 to 2.5, indicating large
173 differences in the simulated magnitude of dust concentrations among climate models.
174 With the validations, we select 5 models for the further analyses including CESM2-
175 WACCM, CNRM-ESM2-1, GFDL-ESM4, NorESM2-LM and UKESM1-0-LL, which
176 yield NSD between 0.25 and 1.5 and correlation coefficients higher than 0.8 against
177 observations.

178 The ensemble median of dust concentrations from 5 selected CMIP6 models is
179 compared to observations at 18 stations (Fig. 2). The models reproduce observed
180 magnitude at 6 sites (Figs 2a–2f) downwind of Saharan dust sources with relative mean
181 biases ranging from –40% to 22%. For these sites, the model ensemble also captures
182 reasonable dust seasonality except for the underestimation of peak values in summer
183 for Barbados (Fig. 2a) and those in spring for Cayenne (Fig. 2b). For the rest sites, the
184 multi-model ensemble prediction overestimates dust concentrations at 1 site in the
185 North Atlantic (Fig. 2g), 3 sites in the southern ocean (Figs 2h–2j), and 3 sites in the



186 central Pacific (Fig. 2k-2m), most of which are far away from dust source regions. In
187 contrast, model simulations underestimate dust concentrations at 1 site in the Indian
188 Ocean (Fig. 2n) and 2 sites at the offshore of East Asia (Figs 2o-2p), likely because
189 climate models underestimate source strength in Middle East and Central Asia. In sum,
190 the simulated dust concentrations show smaller spatial gradients than observations.

191

192 3.2 Dust cycle at present day

193 Based on the selected models, the ensemble median dust emissions, concentrations,
194 and depositions are assessed for 2005-2014 (Fig. 3). About 87% of dust emissions are
195 located in the Northern Hemisphere, with hotspots over North Africa, Middle East, and
196 central Asia and Taklimakan (Fig. 3a). The source intensity is much smaller in the
197 Southern Hemisphere, with moderate emissions over Australia, South Africa, and
198 southern South America. The global total dust emission from the ensemble of models
199 is about 3311 Tg, to which the emissions from Africa alone contribute by 63% (Table
200 3).

201 The spatial distribution of dust deposition resemble that of emissions but with
202 much larger coverage. Dry deposition is usually confined to the source regions (Fig. 3c)
203 because dust particles with large size are more likely to settle down and cannot travel
204 far away from the source. In contrast, wet deposition is more dispersed (Fig. 3d)
205 because small particles can be transported long distances to the downwind areas and
206 finally washed out by rain. On the global scale, the annual total dry deposition is 2463
207 Tg, more than three times of the 815 Tg by wet deposition.

208 The dust budget (emission minus deposition) shows net sources of 376 Tg a⁻¹ in
209 Africa and 71 Tg a⁻¹ in Asia (Table 3). Meanwhile, the ocean acts as a net sink with the
210 largest strength of -262 Tg a⁻¹ in the Atlantic and the secondary of -138 Tg a⁻¹ in the
211 Indian Ocean due to their vicinity to the source regions on the land. Following the
212 emission pattern, dust loading shows high values (>120 mg m⁻²) around the source
213 regions especially North Africa and decreases gradually towards global oceans (Fig.
214 3b).

215

216 3.3 Projection of future dust emissions

217 We calculate the changes of dust emissions at the end of the 21st century (2090-
218 2099) relative to the present day (2005-2014). Global total emissions increase under
219 three scenarios, with the largest change of 53.4 Tg a⁻¹ (1.61%) in the SSP5-8.5 scenario
220 (Fig. 4d). However, the total emissions show a moderate reduction of -15.8 Tg a⁻¹ (-



221 0.48%) in the SSP3-7.0 scenario (Fig. 4c). The most significant changes are located at
222 the major dust source regions, such as North Africa and Middle East. Dust emissions
223 in North Africa increase in all four scenarios, though with regional heterogeneous
224 responses and varied magnitude of 4.2-49.4 Tg a⁻¹ (0.4%-4.7%). The secondary
225 enhancement is found at Australia with increases of 1.0-9.1 Tg a⁻¹ (2.2%-20.7%) under
226 the four scenarios. In contrast, dust emissions in central Asia and Taklimakan show
227 decreases of -0.6 to -18.8 Tg a⁻¹ (-0.6% to -20.0%), which are stronger than the
228 enhancement in North Africa under the SSP3-7.0 scenario (Table 4). Furthermore, dust
229 emissions over Middle East decrease in most scenarios especially for SSP3-7.0, in
230 which the regional reduction dominates the global decline of dust emissions (Fig. 4c).

231 We further explore the associated changes in meteorological conditions at the
232 source regions (Fig. 5). For North America, regional precipitation shows limited
233 changes under all four scenarios because the baseline rainfall is very low (Fig. S1). The
234 ensemble projections show decreased relative humidity of -4.5% to -15.4% and
235 increased surface wind speed of 0.2%-1.8% over North Africa for all scenarios,
236 contributing to the largest enhancement of regional dust emissions. Similarly,
237 projections show decreased precipitation and relative humidity but increased surface
238 wind over South Africa, resulting in the increase of local emissions. As a comparison,
239 precipitation, relative humidity, and surface wind all show decreasing trends in
240 Australia, where the dust emissions increase for all scenarios. It indicates that the effect
241 of drier conditions outweighs the decreased momentum for dust emissions in this
242 specific region. Among the total of 18 regions with increased dust emissions under the
243 four scenarios, 17 show decreased relative humidity by at least 0.5%, 14 show
244 decreased precipitation, and 11 show increase wind speed (Fig. 5).

245 In contrast, the future dust emissions decrease in central Asia, Taklimakan and
246 Middle East under most scenarios (Fig. 4). Climate projections show increased
247 precipitation (Fig. S1) and relative humidity (Fig. S2), but decreased wind speed
248 (Fig.S3) over the source regions in central Asia and Taklimakan. All these changes in
249 meteorological conditions tend to inhibit regional dust mobilization. The most
250 significant reduction of 20.0% occurs in SSP5-8.5 scenario, in which regional
251 precipitation increases by 0.21 mm day⁻¹, and surface wind speed decreases by 0.1 m s⁻¹
252 ¹. For Middle East, relative humidity decreases (Fig. S2) due to limited changes in
253 precipitation (Fig. S1) under the global warming scenarios. However, such tendency is
254 outweighed by the decreased wind speed (Fig. S3), leading to a decline of regional
255 dust emissions in Middle East for most scenarios. Specifically, almost all the 10 regions



256 with reduced dust emissions under the four scenarios show increased regional
257 precipitation but decreased wind speed, though 4 regions (all in Middle East for the
258 four scenarios) show decreased relative humidity (Fig. 5).

259 We select four regions with significant emission changes to quantify the sensitivity
260 of dust emissions to meteorological perturbations (Fig. 6). In these regions, we find
261 positive correlations between the changes in dust emissions and that of wind speed for
262 all models and scenarios. The largest correlation coefficient of 0.8 is derived over North
263 Africa (Fig. 6a). In contrast, both precipitation and relative humidity are negatively
264 correlated with dust emissions across models and scenarios, though such correlations
265 are moderate for relative humidity in central Asia and Taklimakan (Fig. 6f). On average,
266 we derive the increases of dust emissions by 40.5-114.6 Tg per 0.1 m s⁻¹ increase in
267 surface wind (Figs 6a-6d), 8.2-138.7 Tg per 1% reduction in relative humidity (Figs 6e-
268 6h), and 25.6-416.2 Tg per 0.1 mm day⁻¹ reduction in precipitation (Figs 6i-6l) over the
269 main dust source regions based on the multi-model ensemble projections. Following
270 these sensitivities, the inter-model spread of meteorological changes leads to the large
271 uncertainties in the projection of future dust emissions. Among the five climate models,
272 UKESM1-0-LL shows the largest reductions of wind speed while the highest
273 enhancement of precipitation in most of source regions, resulting in the largest decline
274 of dust emission for this model under all the four scenarios (Fig. 6). In contrast, CNRM-
275 ESM2-1 exhibits the largest increase of wind speed and the consequent dust emissions
276 in North Africa. Meanwhile, CESM2-WACCM yields the highest enhancement of dust
277 emissions in Australia where this model projects the largest reduction of precipitation.

278

279 3.4 Projection of future dust loading

280 The dust column concentrations show more continuous changes than dust
281 emissions (Fig. 7). By the end of the 21st century, dust loading increases along the
282 "North Africa-Atlantic-North America" and "Australia-South Africa-South America"
283 belts, but decreases along the "central Asia-East Asia-North Pacific" belt. Such pattern
284 is in general consistent among all four future scenarios with the strongest magnitude
285 under the SSP5-8.5 scenario. The loading in Middle East shows mixed responses with
286 increasing trend in the SSP5-8.5 scenario but decreasing trends in other scenarios. On
287 the global scale, dust loading increases by 0.37-1.65 Tg (2.1%-9.3%) with enhancement
288 of column concentrations in most regions except for Asia and its downwind regions
289 (Fig. 7 and Table S2).

290 We select four dust source regions and two non-source areas in Asia to analyze
291 the driving factors for the changes in dust loading (Fig. 8). Analyses show positive



292 correlation coefficients ranging from 0.79 to 0.92 between dust loading and emissions.
293 In contrast, negative correlations from -0.33 to -0.79 are yielded between the loading
294 and precipitation. The higher magnitude of correlations in the former relationship
295 suggests that the changes of emission dominate the variations of dust loading. However,
296 the role of precipitation cannot be ignored as it can magnify the impact of emissions.
297 For example, dust emissions in the source region of South Africa increase by 2.1%-
298 17.1% under different scenarios (Table 4), while dust loading in this region increases
299 by 2.3%-53.5% (Table S1). The higher enhancement of dust loading than emissions is
300 mainly attributed to the decreased precipitation (Fig. S1), which reduces the proportion
301 of wet deposition to the total deposition (Fig. S4).

302 For the non-source areas such as East Asia and South Asia, the moderate changes
303 of dust emissions cannot explain the significant reductions in dust loading. Instead, the
304 strong enhancement of regional precipitation (Fig. S1) helps promote wet deposition of
305 dust in Asia, leading to the reduced amount of suspended particles (Fig. 7) and the
306 increased percentage of wet-to-total deposition (Fig. S4). Studies have projected that
307 global warming tends to enhance East Asian summer monsoon and South Asian
308 summer monsoon, leading to increased precipitation in the middle and low latitudes of
309 Asia (Sabade et al., 2011; Wang et al., 2018; Wu et al., 2022). These changes are not
310 favorable for regional dust mobilization but tend to decrease dust loading through
311 increased wet deposition.

312

313 **4 Conclusions and discussion**

314 Based on the multi-model ensemble approach, our study projected the changes of
315 dust emissions and loadings by the end of 21st century relative to present day. It is found
316 that dust emissions likely increase in Africa and Australia but decrease in Asia. Such a
317 pattern is consistent among different climate scenarios though the magnitude of
318 regional changes show some variations. As a result, the net changes of global dust
319 emissions vary among future scenarios with the moderate changes in SSP3-7.0 due to
320 the strongest emission reduction over Asia, but the large increase of 4.7% in SSP5-8.5
321 because of the prominent dust emission enhancement in Africa. The changes of dust
322 loading in general follow that of emissions but with associated impacts of precipitation,
323 which magnify the changes of dust loading through less wet deposition over regions
324 with increased emissions (e.g. South Africa) but more deposition over regions with
325 increased precipitation (e.g., East Asia).

326 Our projection revealed large uncertainties in the future global dust cycle. These



327 uncertainties are firstly originated from the discrepancies in the dust emission schemes
328 and the size bins/ranges employed by different climate models. To limit the negative
329 impacts of model diversity, we validated the simulated low-level dust concentrations
330 and selected the models with reasonable performance. The ensemble mean of these
331 selected models could better capture the observed magnitude and distribution of dust
332 concentrations (Fig. 2). However, such validations excluded half of the available
333 models, potentially increasing the uncertainties of multi-model ensemble due to the
334 small sample size. Based on the recent evaluations (Wu et al., 2022; Zhao et al., 2022),
335 the latest version of CMIP models did not improve the performance in the simulated
336 dust cycles, including concentrations, deposition, and optical depth, suggesting that the
337 more validations may rule out even more available models for the future projection. As
338 a result, the observation-based constraint of emission schemes (e.g, adjusting the
339 tunable parameter C in Equation 1) and size bins (e.g., extending or reducing the size
340 range) in individual models is a requisite step to reduce the uncertainties in modeling
341 the global dust cycle.

342 Even though the inter-model variability can not be excluded, we applied the multi-
343 model ensemble approach to minimize the projection biases from individual models.
344 We used the median instead of mean values from the selected models so that our
345 projections reflected the tendency of the majority models rather than that of the single
346 model with maximum changes. At present day, the ensemble projection reasonably
347 captures the observed dust concentrations for most sites. The largest emission from
348 Africa accounts for 63% of the global emissions, similar to the estimates by previous
349 studies (Wu et al., 2020; Aryal and Evans, 2021; Zhao et al., 2022). The global mean
350 burden of 19 Tg is different by -6 Tg to 7 Tg compared to the three datasets used by
351 Zhao et al. (2022). In the future, our ensemble projected increases of dust emissions in
352 North Africa and Australia while the reductions in central Asia are consistent with the
353 results predicted using two different models (Tegen et al., 2004).

354 Our sensitivity analyses showed consistent dependence of dust emissions and
355 loadings to meteorological variables among models and scenarios (Figs 6 and 8). With
356 such physical constraints, the trends of dust emissions are determined by the changes
357 of regional to global meteorological fields, especially wind speed and precipitation. For
358 example, models show contrasting tendencies of surface wind over North Africa (Fig.
359 6a) and precipitation in Australia (Fig. 6l), leading to large inter-model variability with
360 opposite signs for the changes in dust emissions by the end of 21st century. Given the
361 importance of climatic change, we checked the ensemble changes in precipitation (Fig.



362 S5) and surface wind speed (Fig. S6) with all available CMIP6 models (32 models as
363 listed in Table S3) and found that the main features of increased drought and wind speed
364 over North Africa and South Africa while enhanced rainfall over Asia was retained,
365 indicating that the main patterns of the changes in both dust emissions and loadings in
366 our projections are solid. As a result, we suggest that dust emissions over the main
367 source regions will likely enhance in a warming climate, contributing to the increased
368 dust aerosol particles and radiative perturbations by the end of the 21st century.

369

370 **Data availability.** The model output data from CMIP6 were downloaded from
371 <https://esgf-node.llnl.gov/search/cmip6/>.

372

373 **Author contributions.** XY conceived the study. XY and YZ designed the research,
374 conducted the data analysis and paper writing. YaC, JZ, CT and HZ provided paper
375 writing advices and helped with data analysis procedures. YuC, YH, WF and XZ
376 provided scientific advices. All co-authors contributed to improve the manuscript.

377

378 **Competing interests.** The contact author has declared that none of the authors has any
379 competing interests.

380

381 **Acknowledgements.** This research was jointly supported by the Natural Science
382 Foundation of Jiangsu Province (grant no. BK20220031) and the National Natural
383 Science Foundation of China (No. 42275128).

384



385 **References**

- 386 Aryal, Y. N. and Evans, S.: Global Dust Variability Explained by Drought Sensitivity
387 in CMIP6 Models, *J. Geophys. Res.: Earth Surf.*, 126, e2021JF006073, doi:
388 10.1029/2021JF006073, 2021.
- 389 Breuning-Madsen, H. and Awadzi, T. W.: Harmattan dust deposition and particle size
390 in Ghana, *Catena*, 63, 23-38, doi: 10.1016/j.catena.2005.04.001, 2005.
- 391 Csavina, J., Field, J., Félix, O., Corral-Avitia, A. Y., Sáez, A. E., and Betterton, E. A.:
392 Effect of wind speed and relative humidity on atmospheric dust concentrations in
393 semi-arid climates, *Sci. Total Environ.*, 487, 82-90, doi:
394 10.1016/j.scitotenv.2014.03.138, 2014.
- 395 Dunne, J. P., Horowitz, L. W., Adcroft, A. J., Ginoux, P., Held, I. M., John, J. G.,
396 Krasting, J. P., Malyshev, S., Naik, V., Paulot, F., Shevliakova, E., Stock, C. A.,
397 Zadeh, N., Balaji, V., Blanton, C., Dunne, K. A., Dupuis, C., Durachta, J., Dussin,
398 R., Gauthier, P. P. G., Griffies, S. M., Guo, H., Hallberg, R. W., Harrison, M., He,
399 J., Hurlin, W., McHugh, C., Menzel, R., Milly, P. C. D., Nikonov, S., Paynter, D.
400 J., Ploshay, J., Radhakrishnan, A., Rand, K., Reichl, B. G., Robinson, T.,
401 Schwarzkopf, D. M., Sentman, L. T., Underwood, S., Vahlenkamp, H., Winton,
402 M., Wittenberg, A. T., Wyman, B., Zeng, Y., and Zhao, M.: The GFDL Earth
403 System Model Version 4.1 (GFDL - ESM 4.1): Overall Coupled Model
404 Description and Simulation Characteristics, *J. Adv. Model. Earth Syst.*, 12,
405 e2019MS002015, doi: 10.1029/2019MS002015, 2020.
- 406 Evans, S., Ginoux, P., Malyshev, S., and Shevliakova, E.: Climate - vegetation
407 interaction and amplification of Australian dust variability, *Geophys. Res. Lett.*,
408 43, 11823–11830, doi: 10.1002/2016GL071016, 2016.
- 409 Fernandes, R., Dupont, S., and Lamaud, E.: Origins of Turbulent Transport
410 Dissimilarity Between Dust and Momentum in Semiarid Regions, *J. Geophys.*
411 *Res.: Atmos.*, 125, e2019JD031247, doi: 10.1029/2019jd031247, 2020.
- 412 Forster, P., Ramaswamy, V., Artaxo, P., Berntsen, T., Betts, R., Fahey, D. W., Haywood,
413 J., Lean, J., Lowe, D. C., Raga, G., Schulz, M., Dorland, R. V., Bodeker, G.,
414 Etheridge, D., Foukal, P., Fraser, P., Geller, M., Joos, F., Keeling, C. D., Keeling,
415 R., Kinne, S., Lassey, K., Oram, D., O’Shaughnessy, K., Ramankutty, N., Reid,
416 G., Rind, D., Rosenlof, K., Sausen, R., Schwarzkopf, D., Solanki, S. K.,
417 Stenchikov, G., Stuber, N., Takemura, T., Textor, C., Wang, R., Weiss, R., Whorf,
418 T., Nakajima, T., Ramanathan, V., Ramaswamy, V., Artaxo, P., Berntsen, T., Betts,
419 R., Fahey, D. W., Haywood, J., Lean, J., Lowe, D. C., Myhre, G., Nganga, J.,
420 Prinn, R., Raga, G., Schulz, M., and Dorland, R. V.: Changes in Atmospheric
421 Constituents and in Radiative Forcing, *Climate Change 2007: The Physical*
422 *Science Basis*, Cambridge University Press, Cambridge, UK2008.
- 423 Ginoux, P., Chin, M., Tegen, I., Prospero, J. M., Holben, B., Dubovik, O., and Lin, S.-
424 J.: Sources and distributions of dust aerosols simulated with the GOCART model,
425 *J. Geophys. Res.: Atmos.*, 106, 20255-20273, doi: 10.1029/2000JD000053, 2001.
- 426 Goudie, A. S.: Desert dust and human health disorders, *Environ. Int.*, 63, 101-113, doi:
427 10.1016/j.envint.2013.10.011, 2014.
- 428 Jickells, T. D., An, Z. S., Andersen, K. K., Baker, A. R., Bergametti, G., Brooks, N.,



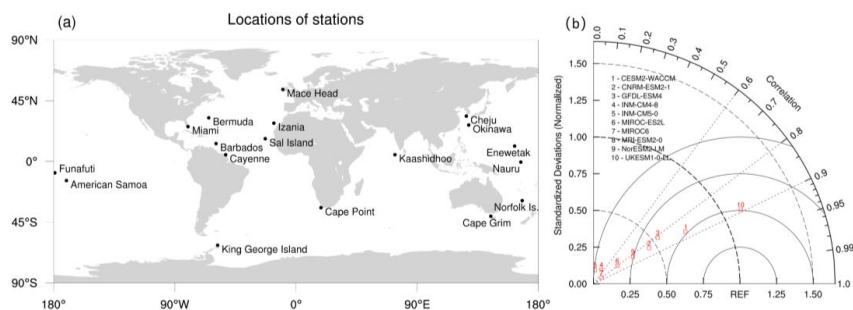
- 429 Cao, J. J., Boyd, P. W., Duce, R. A., Hunter, K. A., Kawahata, H., Kubilay, N.,
430 laRoche, J., Liss, P. S., Mahowald, N., Prospero, J. M., Ridgwell, A. J., Tegen, I.,
431 and Torres, R.: Global Iron Connections Between Desert Dust, Ocean
432 Biogeochemistry, and Climate, *Science*, 308, 67-71, doi:
433 10.1126/science.1105959, 2005.
- 434 Lawrence, D. M., Fisher, R. A., Koven, C. D., Oleson, K. W., Swenson, S. C., Bonan,
435 G., Collier, N., Ghimire, B., Kampenhout, L. v., Kennedy, D., Kluzek, E.,
436 Lawrence, P. J., Li, F., Li, H., Lombardozzi, D., Riley, W. J., Sacks, W. J., Shi, M.,
437 Vertenstein, M., Wieder, W. R., Xu, C., Ali, A. A., Badger, A. M., Bisht, G.,
438 Broeke, M. v. d., Brunke, M. A., Burns, S. P., Buzan, J., Clark, M., Craig, A.,
439 Dahlin, K., Drewniak, B., Fisher, J. B., Flanner, M. G., Fox, A. M., Gentine, P.,
440 Hoffman, F., Keppel-Aleks, G., Knox, R., Kumar, S., Lenaerts, J., Leung, L. R.,
441 Lipscomb, W. H., Lu, Y., Pandey, A., Pelletier, J. D., Perket, J., Randerson, J. T.,
442 Ricciuto, D. M., Sanderson, B. M., Slater, A., Subin, Z. M., Tang, J., Thomas, R.
443 Q., Martin, M. V., and Zeng, X.: The Community Land Model version 5:
444 Description of new features, benchmarking, and impact of forcing uncertainty, *J.*
445 *Adv. Model. Earth Syst.*, 11, 4245-4287, doi: 10.1029/2018MS001583, 2019.
- 446 Li, J., Hao, X., Liao, H., Yue, X., Li, H., Long, X., and Li, N.: Predominant Type of
447 Dust Storms That Influences Air Quality Over Northern China and Future
448 Projections, *Earth's Future*, 10, e2022EF002649, doi: 10.1029/2022ef002649,
449 2022.
- 450 Liu, X., Yin, Z., Zhang, X., and Yang, X.: Analyses of the spring dust storm frequency
451 of northern China in relation to antecedent and concurrent wind, precipitation,
452 vegetation, and soil moisture conditions, *J. Geophys. Res.*, 109, D16210, doi:
453 10.1029/2004JD004615, 2004.
- 454 Mahowald, N. M., Baker, A. R., Bergametti, G., Brooks, N., Duce, R. A., Jickells, T.
455 D., Kubilay, N., Prospero, J. M., and Tegen, I.: Atmospheric global dust cycle and
456 iron inputs to the ocean, *Global Biogeochem. Cycles*, 19, GB4025, doi:
457 10.1029/2004GB002402, 2005.
- 458 Marticorena, B., Bergametti, G., Aumont, B., Callot, Y., N'Doum, C., and Legrand, M.:
459 Modeling the atmospheric dust cycle 2. Simulation of Saharan dust sources, *J.*
460 *Geophys. Res.*, 102, 4387-4404, doi: 10.1029/96JD02964, 1997.
- 461 Middleton, N. J.: Desert dust hazards: A global review, *Aeolian Res.*, 24, 53-63, doi:
462 10.1016/j.aeolia.2016.12.001, 2017.
- 463 Munkhtsetseg, E., Shinoda, M., Gillies, J. A., Kimura, R., King, J., and Nikolich, G.:
464 Relationships between soil moisture and dust emissions in a bare sandy soil of
465 Mongolia, *Particuology*, 28, 131-137, doi: 10.1016/j.partic.2016.03.001, 2016.
- 466 Nabat, P., Somot, S., Mallet, M., Michou, M., Sevault, F., Driouech, F., Meloni, D.,
467 Sarra, A. d., Biagio, C. D., Formenti, P., Sicard, M., Léon, J. F., and Bouin, M. N.:
468 Dust aerosol radiative effects during summer 2012 simulated with a coupled
469 regional aerosol-atmosphere-ocean model over the Mediterranean, *Atmos.*
470 *Chem. Phys.*, 15, 3303-3326, doi: 10.5194/acp-15-3303-2015, 2015.
- 471 Oleson, K. W., Lawrence, D. M., Flanner, M. G., Kluzek, E., Levis, S., Swenson, S. C.,
472 Thornton, E., Dai, A., Decker, M., Dickinson, R., Feddema, J., Heald, C. L.,



- 473 Lamarque, J. F., Niu, G., Qian, T., Running, S., Sakaguchi, K., Slater, A., Stöckli,
474 R., Wang, A., Yang, L., Zeng, X., and Zeng, X.: Technical Description of version
475 4.0 of the Community Land Model (CLM)(No. NCAR/TN-478+STR),
476 University Corporation for Atmospheric Research, 266, 10.5065/D6FB50WZ,
477 2010.
- 478 Penner, J. E., Quaas, J., Storelvmo, T., Takemura, T., Boucher, O., Guo, H., Kirkeva,
479 A., and Seland, Ø.: Model intercomparison of indirect aerosol effects, *Atmos.*
480 *Chem. Phys.*, 6, 3391–3405, doi: 10.5194/acp-6-3391-2006, 2006.
- 481 Pu, B. and Ginoux, P.: How reliable are CMIP5 models in simulating dust optical depth?,
482 *Atmos. Chem. Phys.*, 18, 12491-12510, doi: 10.5194/acp-18-12491-2018, 2018.
- 483 Sabade, S. S., Kulkarni, A., and Kripalani, R. H.: Projected changes in South Asian
484 summer monsoon by multi-model global warming experiments, *Theor. Appl.*
485 *Climatol.*, 103, 543-565, doi: 10.1007/s00704-010-0296-5, 2011.
- 486 Schepanski, K.: Transport of Mineral Dust and Its Impact on Climate, *Geosciences*, 8,
487 151, doi: 10.3390/geosciences8050151, 2018.
- 488 Shao, Y., Wyrwoll, K. H., Chappell, A., Huang, J., Lin, Z., McTainsh, G. H., Mikami,
489 M., Tanaka, T. Y., Wang, X., and Yoon, S.: Dust cycle: An emerging core theme
490 in Earth system science, *Aeolian Res.*, 2, 181-204, doi:
491 10.1016/j.aeolia.2011.02.001, 2011.
- 492 Stefanski, R. and Sivakumar, M. V. K.: Impacts of sand and dust storms on agriculture
493 and potential agricultural applications of a SDSWS, *IOP Conf. Ser.: Earth*
494 *Environ. Sci.*, 7, 012016, doi: 10.1088/1755-1307/7/1/012016, 2009.
- 495 Tegen, I., Werner, M., Harrison, S. P., and Kohfeld, K. E.: Relative importance of
496 climate and land use in determining present and future global soil dust emission,
497 *Geophys. Res. Lett.*, 31, L05105, doi: 10.1029/2003GL019216, 2004.
- 498 Wang, T., Miao, J., Sun, J., and Fu, Y.: Intensified East Asian summer monsoon and
499 associated precipitation mode shift under the 1.5 °C global warming target, *Adv.*
500 *Clim. Change Res.*, 9, 102-111, doi: 10.1016/j.accre.2017.12.002, 2018.
- 501 Wittmann, M., Groot Zwaaftink, C. D., Steffensen Schmidt, L., Guðmundsson, S.,
502 Pálsson, F., Arnalds, O., Björnsson, H., Thorsteinsson, T., and Stohl, A.: Impact
503 of dust deposition on the albedo of Vatnajökull ice cap, Iceland, *The Cryosphere*,
504 11, 741-754, doi: 10.5194/tc-11-741-2017, 2017.
- 505 Woodward, S.: Mineral Dust in HadGEM2, Hadley Centre Technical Note, 087, Met
506 Office Hadley Centre, Fitzroy Road, Exeter, EX1 3PB, United Kingdom.
507 [https://library.metoffice.gov.uk/Portal/Default/en-](https://library.metoffice.gov.uk/Portal/Default/en-GB/RecordView/Index/2522462011)
508 [GB/RecordView/Index/2522462011](https://library.metoffice.gov.uk/Portal/Default/en-GB/RecordView/Index/2522462011).
- 509 Wu, C., Lin, Z., He, J., Zhang, M., Liu, X., Zhang, R., and Brown, H.: A process-
510 oriented evaluation of dust emission parameterizations in CESM: Simulation of
511 a typical severe dust storm in East Asia, *J. Adv. Model. Earth Syst.*, 8, 1432-1452,
512 doi: 10.1002/2016MS000723, 2016.
- 513 Wu, C., Lin, Z., and Liu, X.: The global dust cycle and uncertainty in CMIP5 (Coupled
514 Model Intercomparison Project phase 5) models, *Atmos. Chem. Phys.*, 20, 10401-
515 10425, doi: 10.5194/acp-20-10401-2020, 2020.
- 516 Wu, Q., Li, Q., Ding, Y., Shen, X., Zhao, M., and Zhu, Y.: Asian summer monsoon



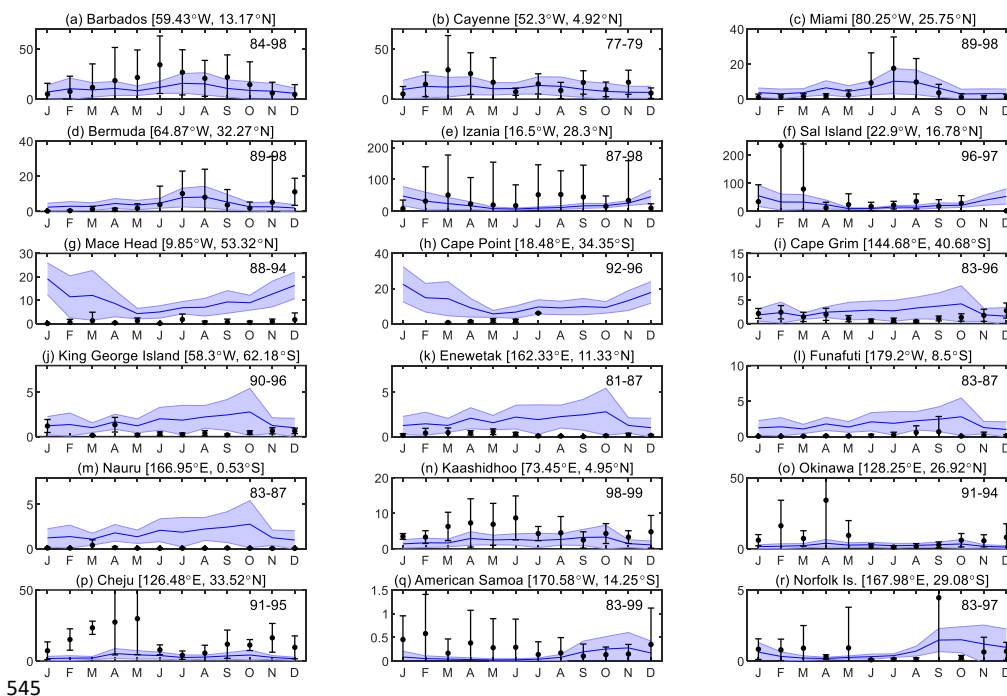
- 517 responses to the change of land–sea thermodynamic contrast in a warming climate:
518 CMIP6 projections, *Adv. Clim. Change Res.*, 13, 205-217, doi:
519 10.1016/j.accre.2022.01.001, 2022.
- 520 Yue, X., Wang, H., Wang, Z., and Fan, K.: Simulation of dust aerosol radiative feedback
521 using the Global Transport Model of Dust: 1. Dust cycle and validation, *J.*
522 *Geophys. Res.*, 114, D10202, doi: 10.1029/2008JD010995, 2009.
- 523 Zakey, A. S., Solmon, F., and Giorgi, F.: Implementation and testing of a desert dust
524 module in a regional climate model, *Atmos. Chem. Phys.*, 6, 4687–4704, doi:
525 10.5194/acp-6-4687-2006, 2006.
- 526 Zhang, D., Gao, X., Zakey, A., and Giorgi, F.: Effects of climate changes on dust aerosol
527 over East Asia from RegCM3, *Adv. Clim. Change Res.*, 7, 145-153, doi:
528 10.1016/j.accre.2016.07.001, 2016.
- 529 Zhang, J., Shao, Y., and Huang, N.: Measurements of dust deposition velocity in a wind-
530 tunnel experiment, *Atmos. Chem. Phys.*, 14, 8869-8882, doi: 10.5194/acp-14-
531 8869-2014, 2014.
- 532 Zhao, A., Ryder, C. L., and Wilcox, L. J.: How well do the CMIP6 models simulate
533 dust aerosols?, *Atmos. Chem. Phys.*, 22, 2095-2119, doi: 10.5194/acp-22-2095-
534 2022, 2022.
- 535 Zong, Q., Mao, R., Gong, D., Wu, C., Pu, B., Feng, X., and Sun, Y.: Changes in Dust
536 Activity in Spring over East Asia under a Global Warming Scenario, *Asia-Pac. J.*
537 *Atmos. Sci.*, 57, 839-850, doi: 10.1007/s13143-021-00224-7, 2021.
- 538
- 539



540

541 **Figure 1.** (a) Locations of 18 observation stations in the University of Miami Ocean
542 Aerosol Network and the (b) evaluation of simulated dust concentrations from CMIP6
543 models at these stations.

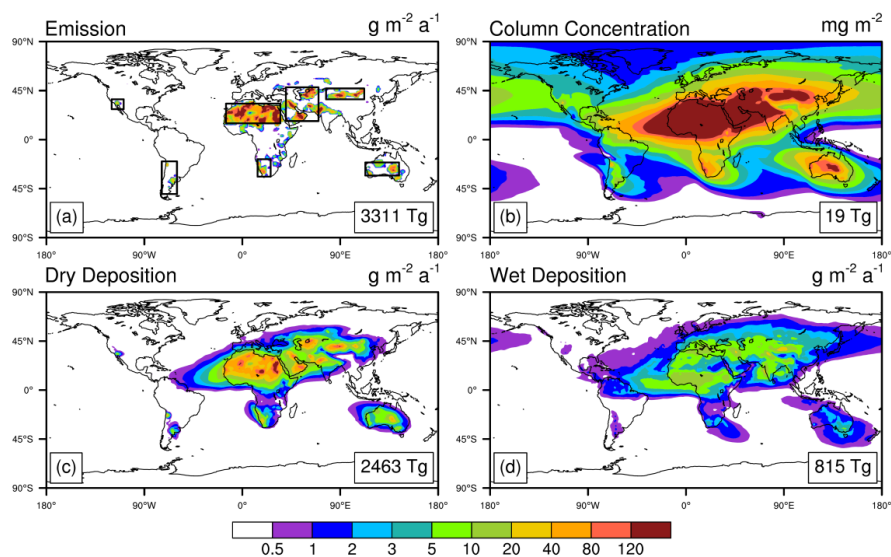
544



545

546 **Figure 2.** Comparison of monthly dust concentrations (units: $\mu\text{g m}^{-3}$) between ensemble
547 simulations by CMIP6 models and observations at 18 sites. The solid lines represent
548 ensemble mean of simulations with shadows indicating inter-model spread. The points
549 are the monthly mean of observations with errorbars indicating year-to-year variability.
550 The time span of observations at each site is shown in the upper right corner of each
551 panel.

552



553

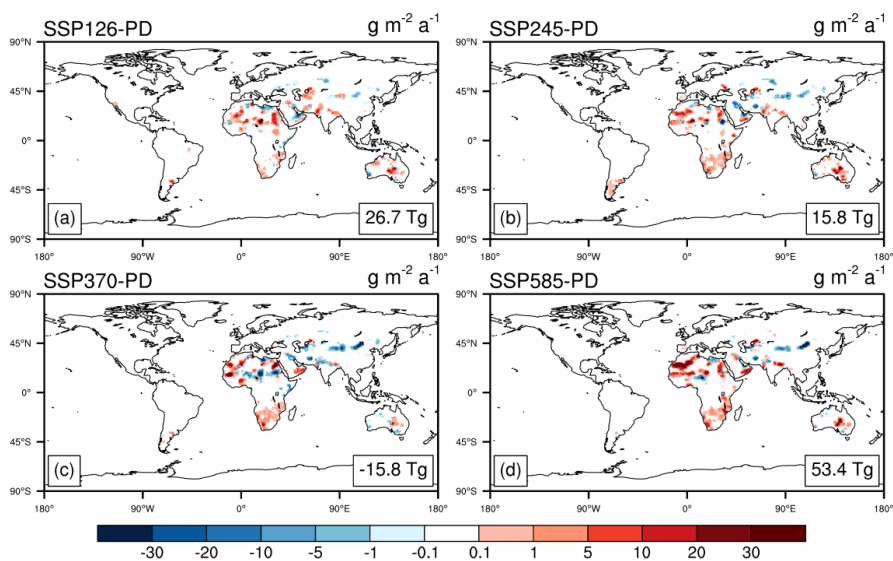
554 **Figure 3.** Multi-model ensemble of (a) emissions, (b) column concentration, (c) dry
555 deposition, and (d) wet deposition of dust aerosols at present day (2005-2014). The box
556 regions on (a) are dust sources of North Africa (NAF), Middle East (MEA), central
557 Asia and Taklimakan (CAT), Australia (AUS), North America (NAM), South America
558 (SAM), and South Africa (SAF). The detailed results for individual models are shown
559 in Fig. S7.

560

561

562

563



564

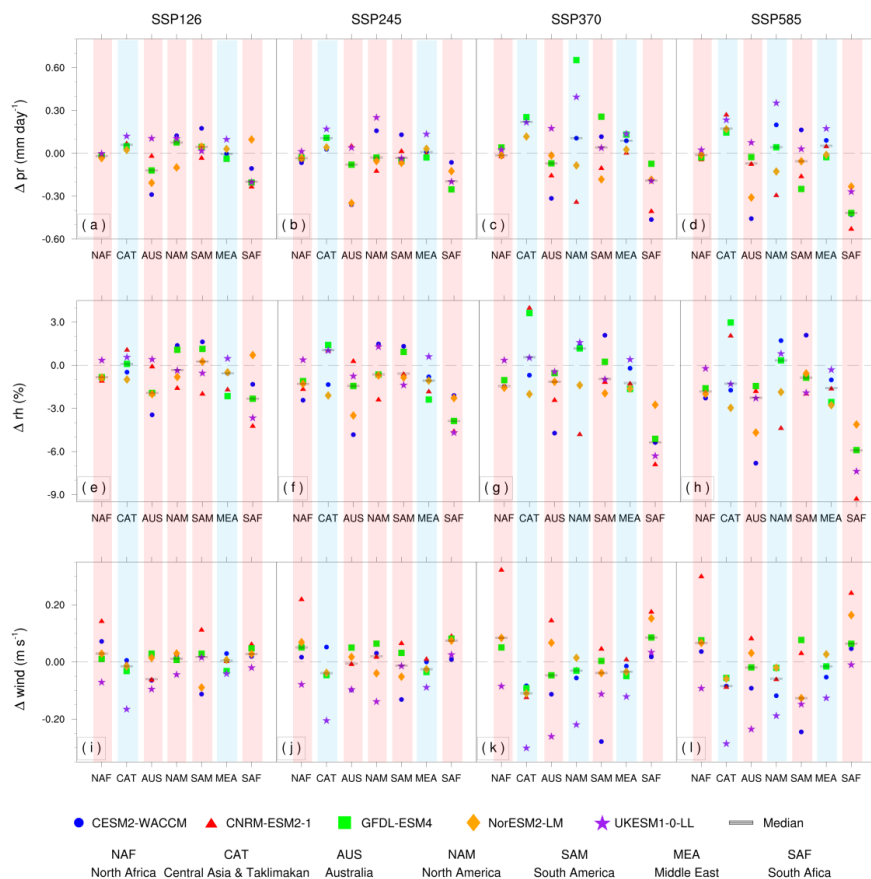
565 **Figure 4.** Multi-model ensemble projection of the changes in dust emissions by the end
566 of 21st century (2090-2099) relative to present day (2005-2014) under four different
567 anthropogenic emission scenarios. The detailed projections at 2090-2099 for individual
568 models are shown in Fig. S8-S11 under four different scenarios.

569

570

571

572

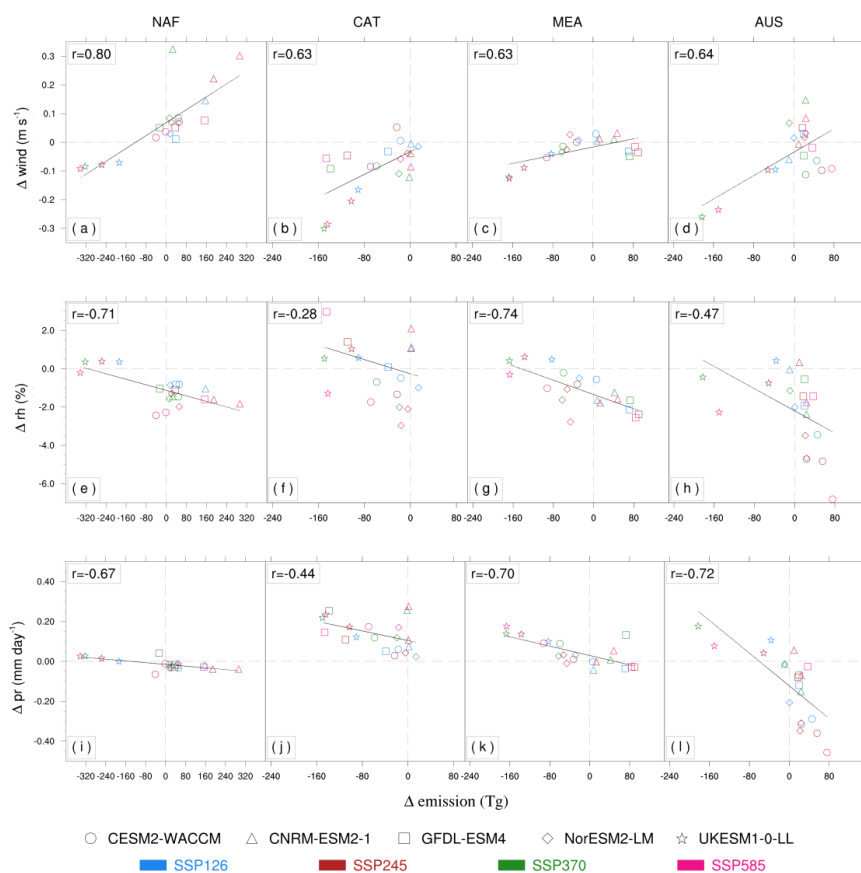


573

574 **Figure 5.** Changes of meteorological factors over main dust emission regions under
 575 four SSP scenarios by the end of 21st century (2090-2099) relative to present day (2005-
 576 2014). Each box column represents a future climate scenario, including SSP1-2.6,
 577 SSP2-4.5, SSP3-7.0 and SSP5-8.5. Each row represents a meteorological factor,
 578 including precipitation (top), relative humidity (middle), and surface wind (bottom).
 579 Regions with emissions increasing are marked with red bars, while regions with
 580 emissions decreasing are marked with blue bars.

581

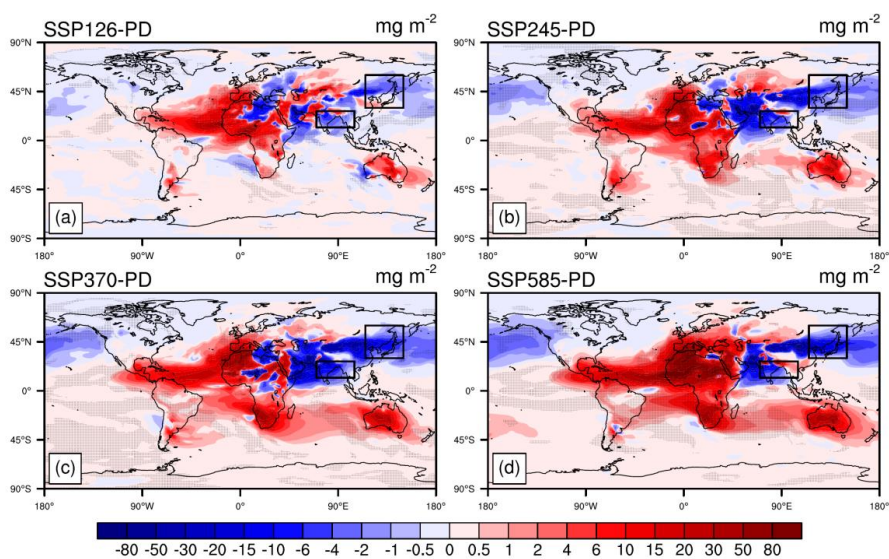
582



583

584 **Figure 6.** Relationships between the changes of dust emissions and the changes of
 585 meteorological factors. Each column represents a source region, including North Africa
 586 (NAF), central Asia and Taklimakan (CAT), Middle East (MEA), and Australia (AUS).
 587 Each row represents a meteorological factor, including surface wind (top), relative
 588 humidity (middle), and precipitation (bottom).

589



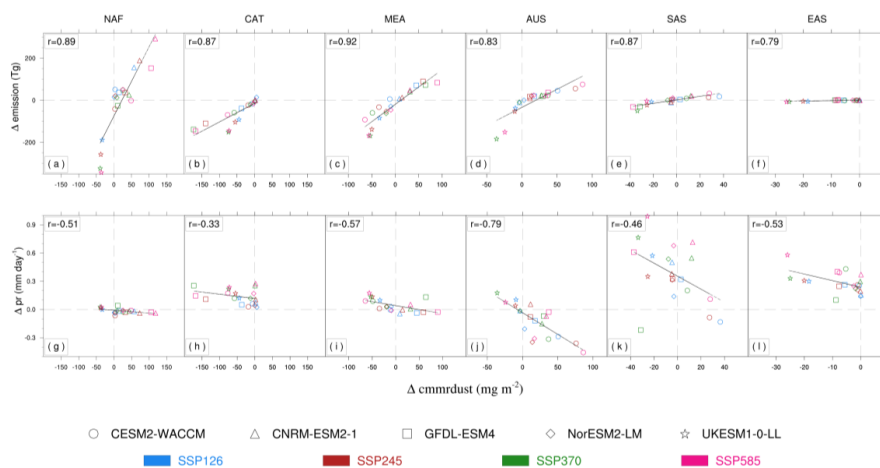
590

591 **Figure 7.** Multi-model ensemble projection of the changes in dust column
592 concentrations by the end of 21st century (2090-2099) relative to present day (2005-
593 2014). Dotted areas represent changes significant at 90% level. Two additional box
594 areas are selected for South Asia and East Asia.

595

596

597



598

599 **Figure 8.** Relationships between the changes of dust column concentrations and the
600 change of influencing factors. From left to right, each column represents a specific
601 region including North Africa (NAF), central Asia and Taklimakan (CAT), Middle East
602 (MEA), Australia (AUS), South Asia (SAS) and East Asia (EAS). Each row represents
603 an influencing factor, including dust emissions (top) and precipitation (bottom).

604

605

606



607

Table 1. The information of CMIP6 models

Model ^a	Nation	Resolution
CESM2-WACCM	U.S.	1.25°×0.94°
CNRM-ESM2-1	France	1.4°×1.4°
GFDL-ESM4	U.S.	1.25°×1°
INM-CM4-8	Russia	2°×1.5°
INM-CM5-0	Russia	2°×1.5°
MIROC-ES2L	Japan	2.8°×2.8°
MIROC6	Japan	1.4°×1.4°
MRI-ESM2-0	Japan	1°×1°
NorESM2-LM	Norway	2°×2°
UKESM1-0-LL	U.K.	1.875°×1.25°

608

609 ^a The models selected for future projections are bolded.

610



611 **Table 2.** The parameterization schemes of dust emission function

Model	E	M_i	f_m	%clay	Reference
CESM2- WACCM	$U_f^3 \left(1 - \frac{U_t}{U_f}\right) \left(1 + \frac{U_t}{U_f}\right)^2$	3 source modes, 4 dust bins	Fraction of grid cell excluding snow, lake and vegetation; depends on liquid water and ice contents in top soil layer	Used to calculate the sandblasting mass efficiency and U_t	Oleson et al. (2010) Wu et al. (2016)
NorESM2- LM					
UKESM1- 0-LL	$U_f^3 \left(1 + \frac{U_t}{U_f}\right) \left(1 - \left(\frac{U_t}{U_f}\right)^2\right)$	9 dust bins	Considering grid cell fractions of vegetation		Woodward, (2011)
CNRM- ESM2-1		3 dust bins	Using roughness length	Used to calculate the U_t	Marticorena et al. (1997) Zakey et al. (2006) Nabat et al. (2015)
GFDL- ESM4	$U_f^2 (U_f - U_t)$	5 dust bins	Using leaf area index and stem area index	/	Evans et al. (2016) Dunne et al. (2020)

612

613

614



615

616

Table 3. The summary of dust cycle at present day

Region	Emission	Dry Deposition	Wet Deposition	Budget*
	Tg a ⁻¹	Tg a ⁻¹	Tg a ⁻¹	Tg a ⁻¹
Africa	2171	1541	254	376
Asia	893	591	231	71
Australia	255	182	27	45
South America	80	47	22	11
North America	26	20	9	-2
Europe	6	14	32	-40
the Pacific Ocean	/	14	43	-57
the Indian Ocean	/	61	77	-138
the Atlantic Ocean	/	115	147	-262
the Arctic Ocean	/	0.3	2.1	-2.4

617

*Budget = Emission - Dry Deposition - Wet Deposition

618

619

620

621

622



623 **Table 4.** Multi-model ensemble projection of the absolute (Tg a^{-1}) and relative
624 changes (%) in dust emissions by the end of this century (2090-2099)

Region	SSP1-2.6		SSP2-4.5		SSP3-7.0		SSP5-8.5	
	Absolute	Relative	Absolute	Relative	Absolute	Relative	Absolute	Relative
NAF	19.1	1.8	10.3	1.0	4.2	0.4	49.4	4.7
CAT	-0.6	-0.6	-5.1	-5.4	-17.7	-18.8	-18.8	-20.0
MEA	-0.6	-0.2	-6.2	-2.5	-6.9	-2.8	-0.1	0.0
AUS	3.8	8.7	9.1	20.7	1.0	2.2	8.7	19.9
NAM	0.1	3.1	0.0	0.4	0.0	-1.4	0.0	-1.2
SAM	1.1	14.9	0.7	10.4	0.3	4.6	0.0	0.6
SAF	0.6	2.1	0.8	3.0	4.5	17.1	3.9	14.6

625 * The scope of each region is shown in Figure 1a

626

627

628